Supplementary Figure 1

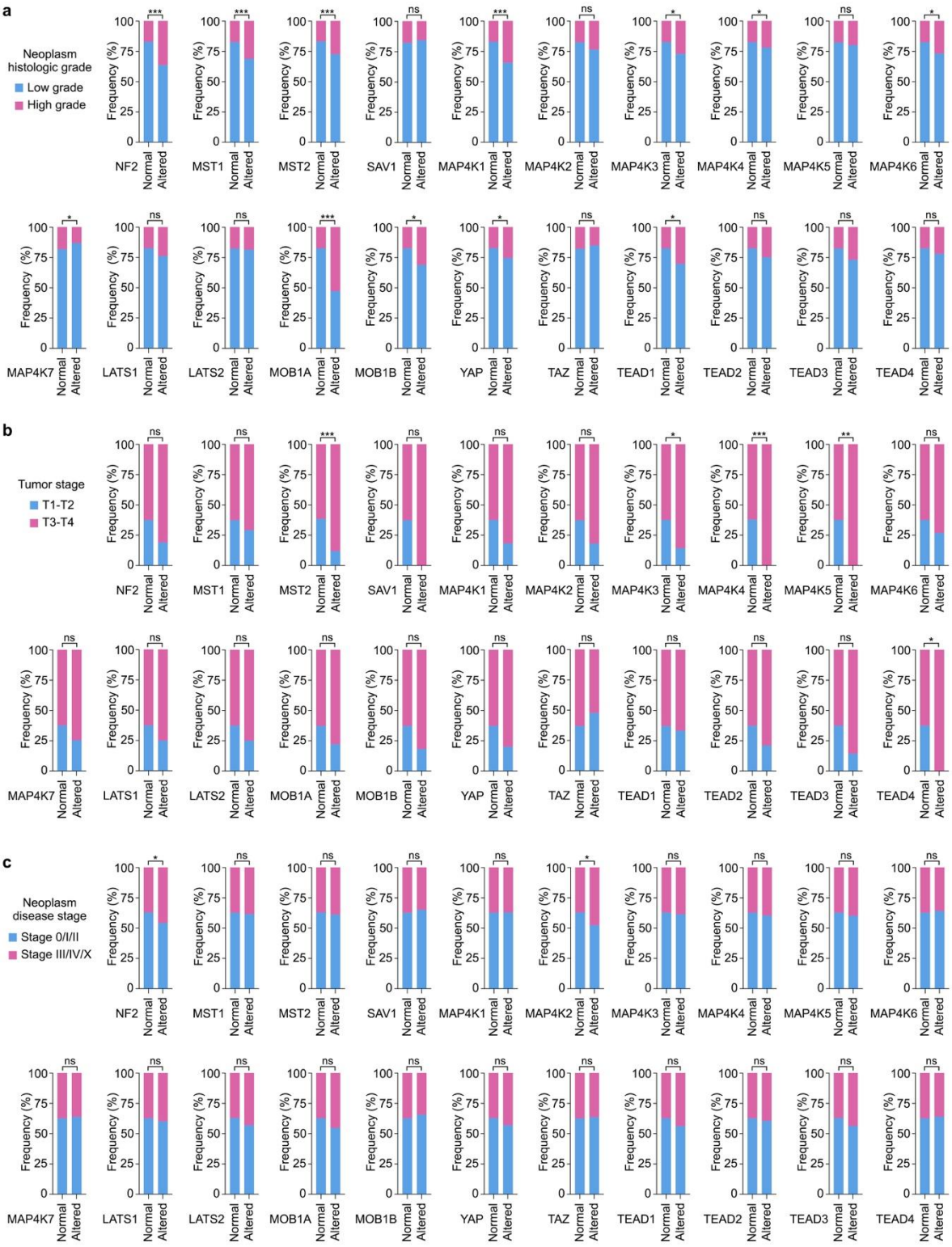

**Supplementary Figure 1. Histological analysis of cancer patient samples with individual altered Hippo signaling genes.**

(**a-c**) Tumor samples with normal and altered Hippo signaling genes are analyzed for their neoplasm histologic grade (**a**), tumor stage (**b**), and neoplasm disease stage (**c**). ns, no significance. * $p < 0.05$, ** $p < 0.01$, *** $p < 0.001$ (Chi-squared test). Source data are provided as a Source Data file.

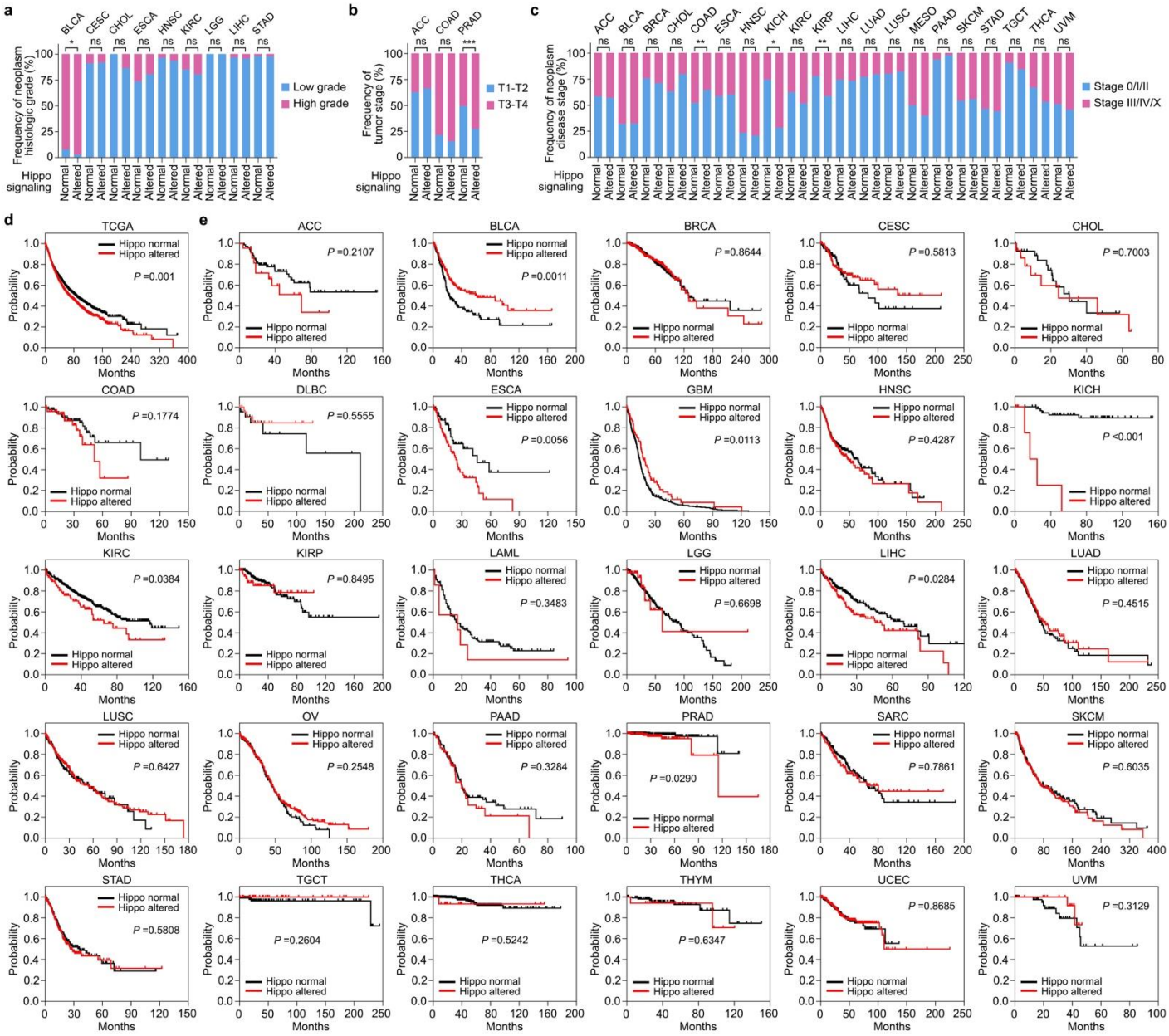
a
b
c
Frequency of neoplasm histologic grade (%)
Low grade
High grade
Frequency of tumor stage (%)
T1-T2
T3-T4
Frequency of neoplasm disease stage (%)
Stage 0/I/II
Stage III/IV/X
Hippo signaling
Normal
Altered
d
e
TCGA
ACC
BLCA
BRCA
CESC
CHOL
COAD
DLBC
ESCA
GBM
HNSC
KICH
KIRC
KIRP
LAML
LGG
LIHC
LUAD
LUSC
OV
PAAD
PRAD
SARC
SKCM
STAD
TGCT
THCA
THYM
UCEC
UVM
Probability
Months
Hippo normal
Hippo altered

**Supplementary Figure 2. Histological and survival analyses of cancer patients with altered Hippo signaling genes in different cancer types.**

(**a-c**) Tumor samples with normal and altered Hippo signaling genes are analyzed for their neoplasm histologic grade (**a**), tumor stage (**b**), and neoplasm disease stage (**c**) in different cancer types. ns, no significance. * $p < 0.05$, ** $p < 0.01$, *** $p < 0.001$ (Chi-squared test).

(**d-e**) Overall survival analysis of cancer patients with normal and altered Hippo signaling genes. The overall survival of cancer patients with normal and altered Hippo signaling genes in TCGA (**d**) and the indicated cancer types (**e**) was analyzed using log-rank (Mantel-Cox) test.

Source data are provided as a Source Data file.

Supplementary Figure 3

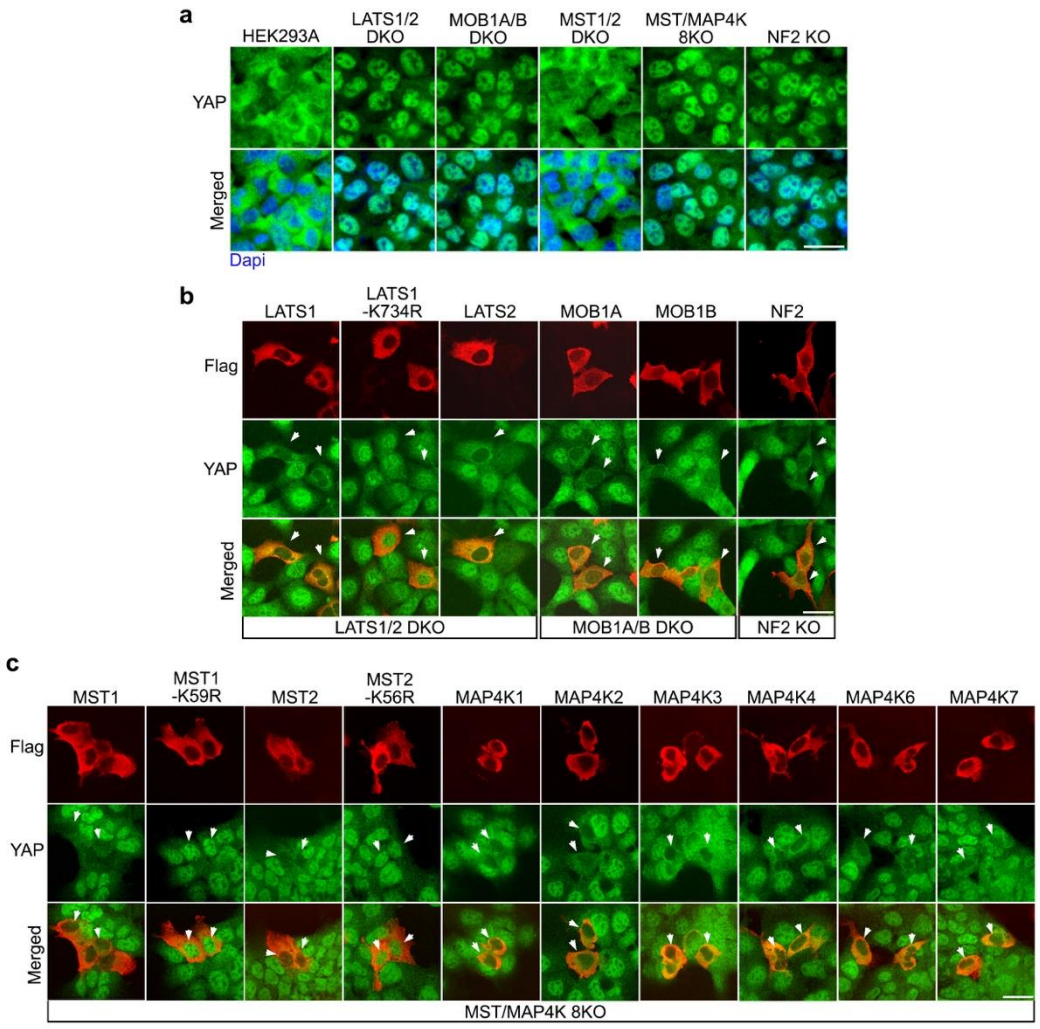

**Supplementary Figure 3. Validation of Hippo pathway gene knockout (KO) cells for missense mutation screen.**

(**a**) YAP is enriched the nucleus of the LATS1/2 double KO (DKO), MOB1A/B DKO, MST/MAP4K-8KO, and NF2 KO HEK293A cells. The indicated Hippo component KO HEK293A cells were subjected to immunofluorescent staining. Nucleus was visualized by Dapi. Scale bar, 20 μm.

(**b-c**) Validation of the Hippo component KO HEK293A cells. The indicated LATS1/2 DKO (**b**), MOB1A/B DKO (**b**), NF2 KO (**b**), and MST/MAP4K-8KO (**c**) HEK293A cells were transfected with the indicated constructs and subjected to immunofluorescent staining. Scale bar, 30 μm. Arrows showed the cells expressing the indicated constructs.

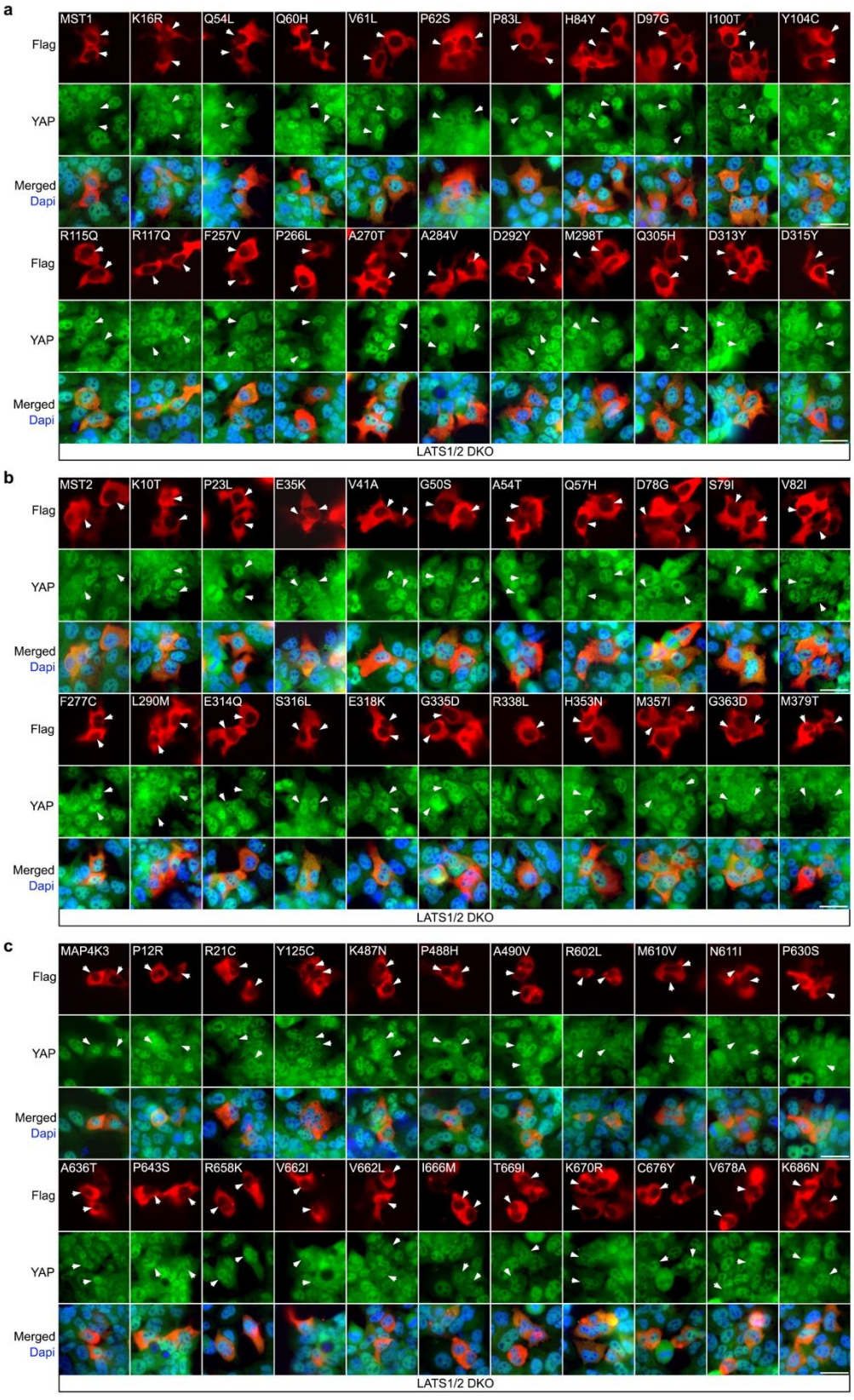
a
MST1
K16R
Q54L
Q60H
V61L
P62S
P83L
H84Y
D97G
I100T
Y104C
Flag
YAP
Merged
Dapi
R115Q
R117Q
F257V
P266L
A270T
A284V
D292Y
M298T
Q305H
D313Y
D315Y
LATS1/2 DKO
b
MST2
K10T
P23L
E35K
V41A
G50S
A54T
Q57H
D78G
S79I
V82I
F277C
L290M
E314Q
S316L
E318K
G335D
R338L
H353N
M357I
G363D
M379T
c
MAP4K3
P12R
R21C
Y125C
K487N
P488H
A490V
R602L
M610V
N611I
P630S
A636T
P643S
R658K
V662I
V662L
I666M
T669I
K670R
C676Y
V678A
K686N

**Supplementary Figure 4. Characterization of the neutral mutations of MST1, MST2 and MAP4K3 in the LATS1/2 DKO cells.**

(**a-c**) The LATS1/2 DKO HEK293A cells were transfected with the indicated neutral missense mutants of MST1 (**a**), MST2 (**b**), and MAP4K3 (**c**) and subjected to immunofluorescent staining. Scale bar, 30 μm. Arrows showed the cells expressing the indicated constructs.

Supplementary Figure 5

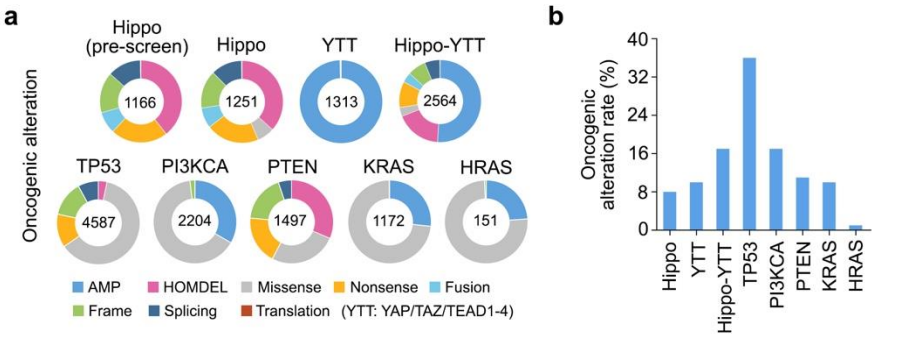


**Supplementary Figure 5. Analysis of the Hippo signaling oncogenic alterations.**

(**a**) The oncogenic alterations of Hippo signaling genes and the indicated tumor suppressor genes and oncogenes were summarized. The number of affected cancer patients was indicated.

(**b**) The oncogenic alteration rates for Hippo signaling genes and the indicated cancer-related genes were shown.

Source data are provided as a Source Data file.

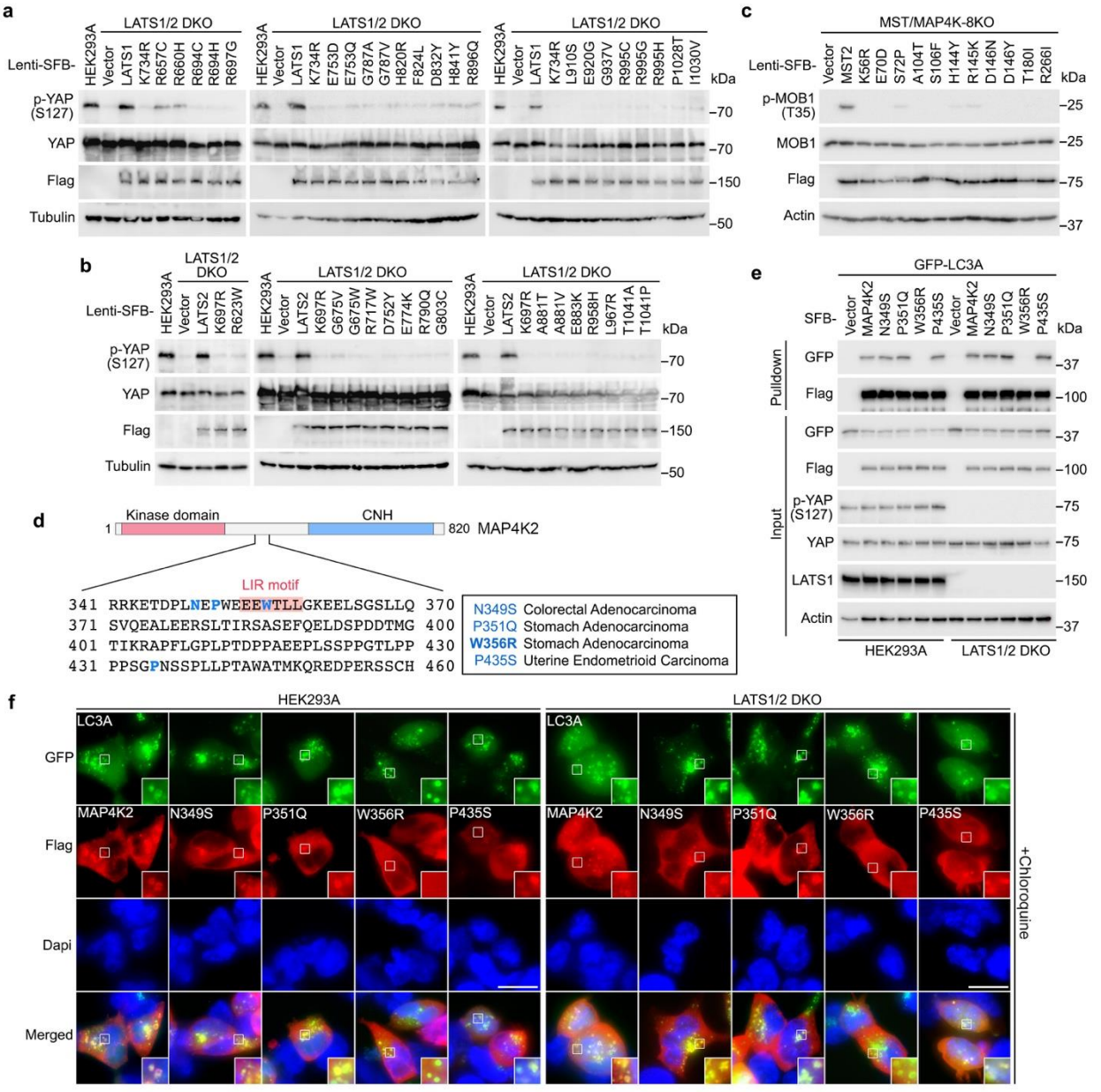
a
LATS1/2 DKO
Lenti-SFB-
HEK293A
Vector
LATS1
K734R
R657C
R660H
R694C
R694H
R697G
E753D
G787A
G787V
H820R
F824L
D832Y
H841Y
R896Q
L910S
E920G
G937V
R995C
R995G
R995H
P1028T
I1030V
kDa
p-YAP (S127)
YAP
Flag
Tubulin
–70
–150
–50
b
LATS1/2 DKO
LATS2
K697R
R623W
G675V
G675W
R717W
D752Y
E774K
R790Q
G803C
A881T
A881V
E883K
R958H
L967R
T1041A
T1041P
c
MST/MAP4K-8KO
MST2
K56R
E70D
S72P
A104T
S106F
H144Y
R145K
D146N
D146Y
T180I
R266I
p-MOB1 (T35)
MOB1
Actin
–25
–75
–37
d
Kinase domain
CNH
1
820
MAP4K2
LIR motif
341 RRKETDPLNEPWEEEWTLLGKEELSGSLLQ 370
371 SVQEALEERSLTIRSASEFQELDSPDDTMG 400
401 TIKRAPFLGPLPTDPPAEEPLSSPPGTLPP 430
431 PPSGPNSSPLLPTAWATMKQREDPERSSCH 460
N349S Colorectal Adenocarcinoma
P351Q Stomach Adenocarcinoma
W356R Stomach Adenocarcinoma
P435S Uterine Endometrioid Carcinoma
e
GFP-LC3A
SFB-
MAP4K2
N349S
P351Q
W356R
P435S
Pulldown
Input
GFP
Flag
p-YAP (S127)
YAP
LATS1
Actin
–100
HEK293A
LATS1/2 DKO
f
HEK293A
LATS1/2 DKO
LC3A
GFP
MAP4K2
N349S
P351Q
W356R
P435S
Flag
Dapi
Merged
+Chloroquine

**Supplementary Figure 6. Characterization of the Hippo LOF and neutral missense mutations.**

(**a-b**) Analysis of LATS1/2 LOF missense mutations in stable cells. The LATS1/2 DKO HEK293A cells stably expressing the indicated LOF mutants of LATS1 (**a**) and LATS2 (**b**) were subjected to Western blot. A representative blot of two independent experiments is shown.

(**c**) Analysis of MST2 LOF missense mutations in stable cells. The MST/MAP4K-8KO HEK293A cells stably expressing the indicated MST2 LOF mutants were subjected to Western blot. A representative blot of two independent experiments is shown.

(**d**) The MAP4K2 neutral mutation W356R is identified in its LIR motif. W356R and its nearby neutral mutations were indicated in blue. The LIR motif was highlighted in red.

(**e**) The W356R neutral mutation disrupted the interaction of MAP4K2 with LC3A in both wild-type and LATS1/2 DKO HEK293A cells. Wild-type and LATS1/2 DKO HEK293A cells were transfected with GFP-LC3A and the indicated SFB-MAP4K2 constructs and subjected to pulldown assay using S protein beads. A representative blot of two independent experiments is shown.

(**f**) The W356R neutral mutation disrupted the co-localization of MAP4K2 with LC3A in chloroquine-treated wild-type and LATS1/2 DKO HEK293A cells. The constructs encoding GFP-LC3A and the indicated SFB-MAP4K2 mutants were co-expressed in wild-type and LATS1/2 DKO HEK293A cells, treated with chloroquine (200 μM) for 4 hours, and subjected to immunofluorescent staining. The indicated regions in the box are shown 3 times enlarged. Scale bar, 20 μm.

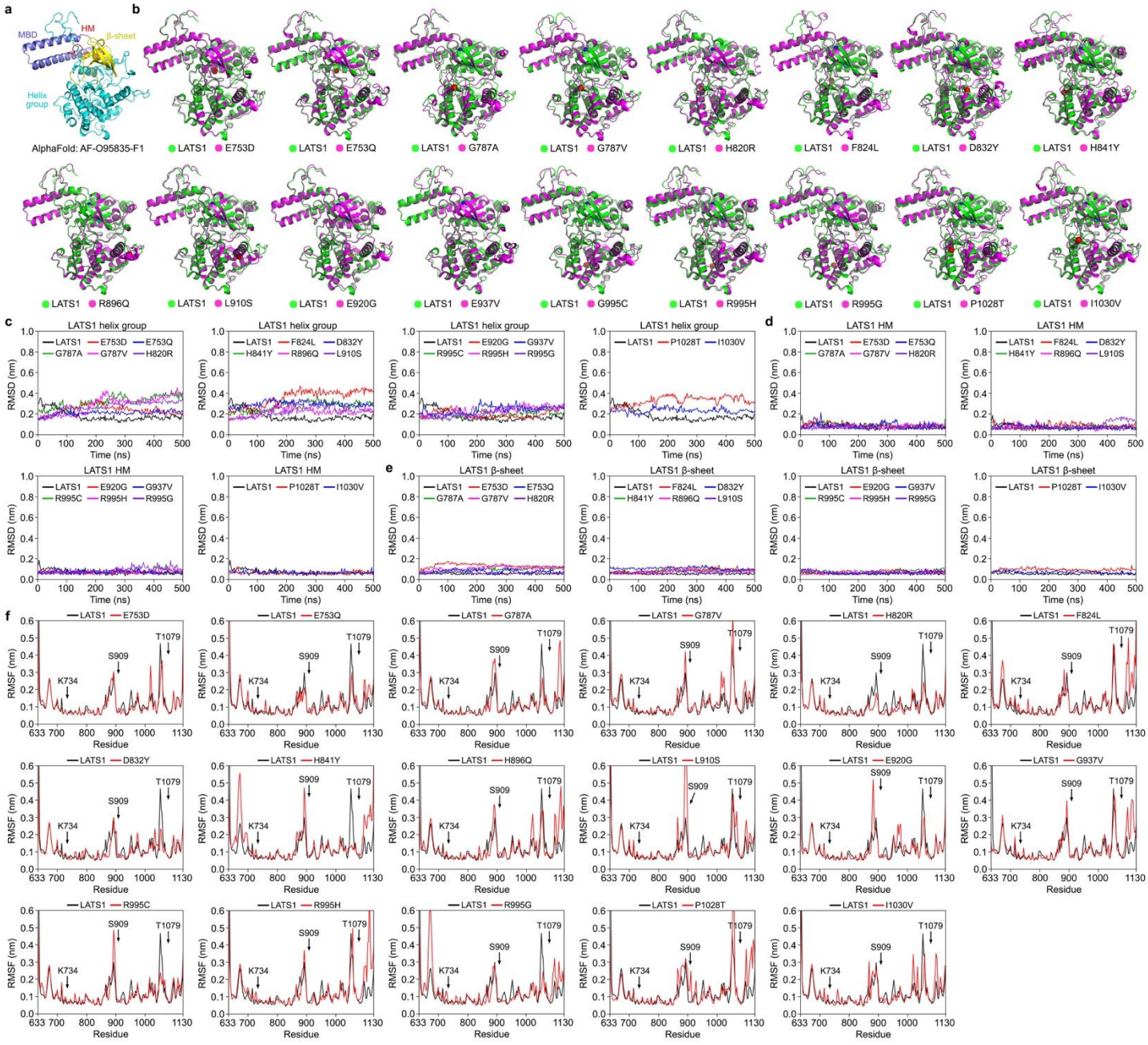
a
MBD
HM
β-sheet
Helix group
AlphaFold: AF-O95835-F1
b
LATS1 E753D
LATS1 E753Q
LATS1 G787A
LATS1 G787V
LATS1 H820R
LATS1 F824L
LATS1 D832Y
LATS1 H841Y
LATS1 R896Q
LATS1 L910S
LATS1 E920G
LATS1 E937V
LATS1 G995C
LATS1 R995H
LATS1 R995G
LATS1 P1028T
LATS1 I1030V
c
LATS1 helix group
LATS1 HM
d
LATS1 HM
e
LATS1 β-sheet
RMSD (nm)
Time (ns)
f
RMSF (nm)
Residue
K734
S909
T1079

**Supplementary Figure 7. Molecular dynamics analysis of the LATS1 LOF missense mutations.**

(**a**) The LATS1 protein structure including its MOB1-binding domain (MBD) and kinase domain (predicted using AlphaFold2) is used for the molecular dynamics analysis. The MBD, helix group, hydrophobic motif (HM), and β-sheet were shown in different colors.

(**b**) The LATS1 LOF missense mutations induce its protein conformational change. The overlay structures were shown for LATS1 and its indicated LOF missense mutants.

(**c**-**e**) RMSD analysis is performed to examine the LATS1 LOF missense mutations-caused effects on its kinase domain structure, where LATS1 helix group (**c**), HM (**d**), and β-sheet (**e**) were examined.

(**f**) RMSF analysis is performed for the LATS1 kinase domain LOF missense mutants. LATS1 ATP-binding site K734, autophosphorylation site S909, and HM phosphorylation site T1079 were indicated.

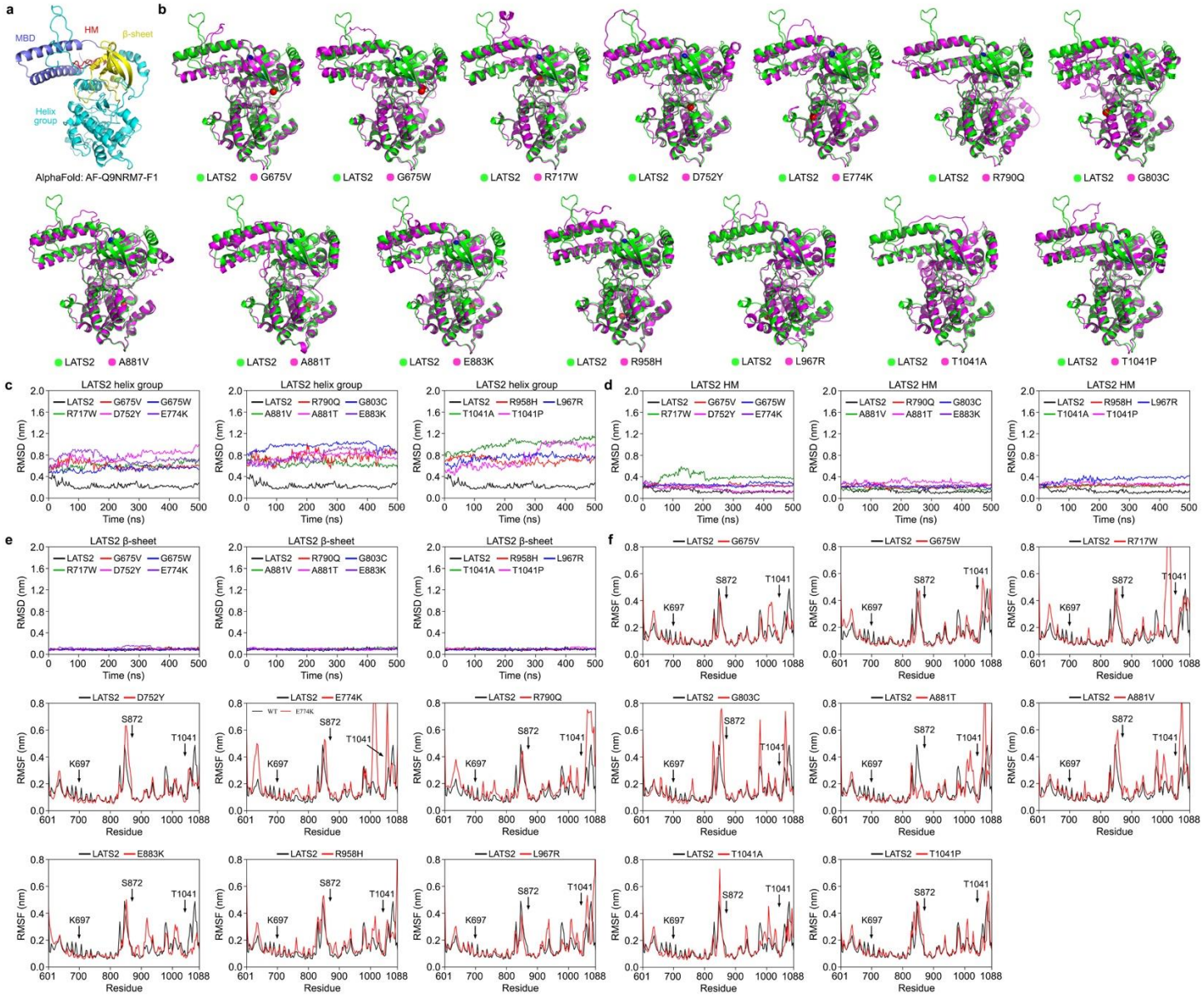
a
MBD
HM
β-sheet
Helix group
AlphaFold: AF-Q9NRM7-F1
b
LATS2 G675V
LATS2 G675W
LATS2 R717W
LATS2 D752Y
LATS2 E774K
LATS2 R790Q
LATS2 G803C
LATS2 A881V
LATS2 A881T
LATS2 E883K
LATS2 R958H
LATS2 L967R
LATS2 T1041A
LATS2 T1041P
c
LATS2 helix group
d
LATS2 HM
RMSD (nm)
Time (ns)
e
LATS2 β-sheet
f
RMSF (nm)
Residue
K697
S872
T1041
WT
E774K

**Supplementary Figure 8. Molecular dynamics analysis of the LATS2 LOF missense mutations.**

(**a**) The LATS2 protein structure including its MOB1-binding domain (MBD) and kinase domain (predicted using AlphaFold2) is used for the molecular dynamics analysis. The MBD, helix group, hydrophobic motif (HM), and β-sheet were shown in different colors.

(**b**) The LATS2 LOF missense mutations induce its protein conformational change. The overlay structures were shown for LATS2 and its indicated LOF missense mutants.

(**c**-**e**) RMSD analysis is performed to examine the LATS2 LOF missense mutations-caused effects on its kinase domain protein structure, where LATS2 helix group (**c**), HM (**d**), and β-sheet (**e**) were examined.

(**f**) RMSF analysis is performed for the LATS2 kinase domain LOF missense mutants. LATS2 ATP-binding site K697, autophosphorylation site S872, and HM phosphorylation site T1041 were indicated.

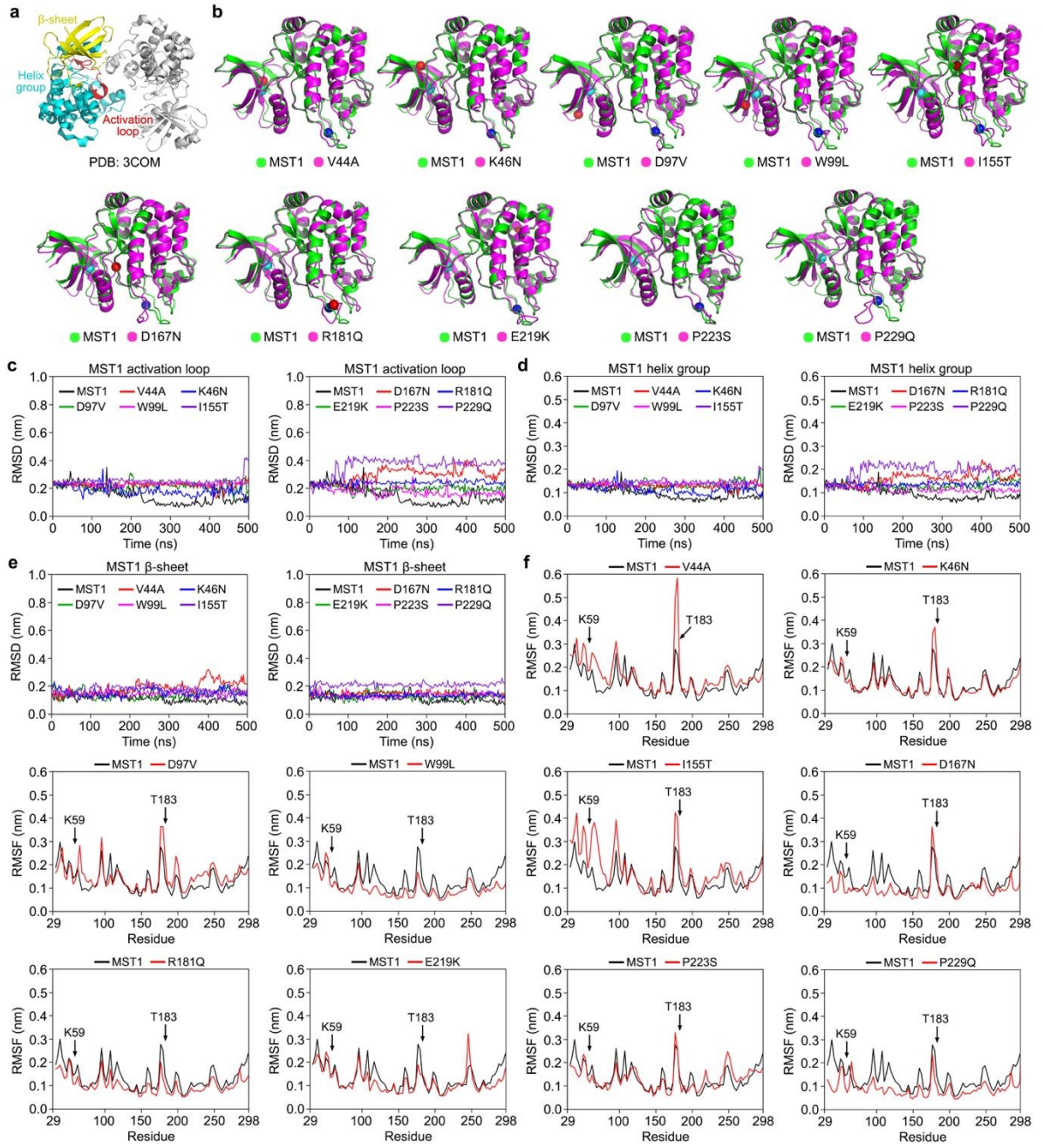
a
β-sheet
Helix group
Activation loop
PDB: 3COM
b
MST1 V44A
MST1 K46N
MST1 D97V
MST1 W99L
MST1 I155T
MST1 D167N
MST1 R181Q
MST1 E219K
MST1 P223S
MST1 P229Q
c
MST1 activation loop
RMSD (nm)
Time (ns)
d
MST1 helix group
e
MST1 β-sheet
f
RMSF (nm)
Residue
K59
T183

**Supplementary Figure 9. Molecular dynamics analysis of the MST1 LOF missense mutations.**

(**a**) The MST1 kinase domain protein structure (PDB: 3COM) is used for the molecular dynamics analysis. The activation loop, helix group, and β-sheet were shown in different colors.

(**b**) The MST1 LOF missense mutations induce its kinase domain conformational change. The kinase domain overlay structures were shown for MST1 and its LOF missense mutants.

(**c-e**) RMSD analysis is performed to examine the MST1 LOF missense mutations-caused effects on its kinase domain protein structure, where MST1 kinase domain activation loop (**c**), helix group (**d**), and β-sheet (**e**) were examined.

(**f**) RMSF analysis is performed for the MST1 kinase domain LOF missense mutants. MST1 ATP-binding site K59 and autophosphorylation site T183 were indicated.

Supplementary Figure 10

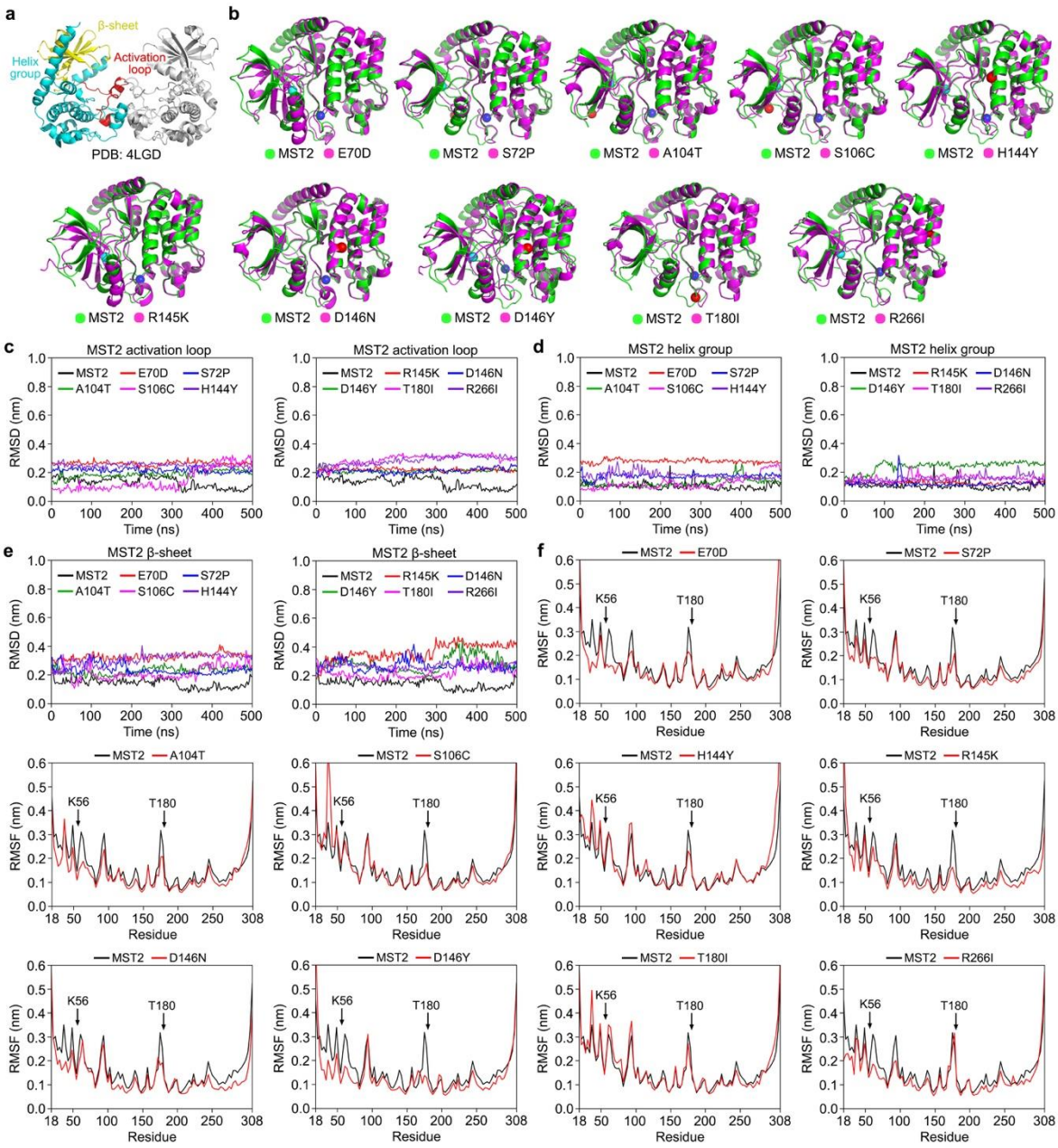

**Supplementary Figure 10. Molecular dynamics analysis of the MST2 LOF missense mutations.**

(**a**) The MST2 kinase domain protein structure (PDB: 4LGD) is used for the molecular dynamics analysis. The activation loop, helix group, and β-sheet were shown in different colors.

(**b**) The MST2 LOF missense mutations induce its kinase domain conformational change. The kinase domain overlay structures were shown for MST2 and its indicated LOF missense mutants.

(**c-e**) RMSD analysis is performed to examine the MST2 LOF missense mutations-caused effects on its kinase domain protein structure, where MST2 kinase domain activation loop (**c**), helix group (**d**), and β-sheet (**e**) were examined.

(**f**) RMSF analysis is performed for the MST2 kinase domain LOF missense mutants. MST2 ATP-binding site K56 and autophosphorylation site T180 were indicated.

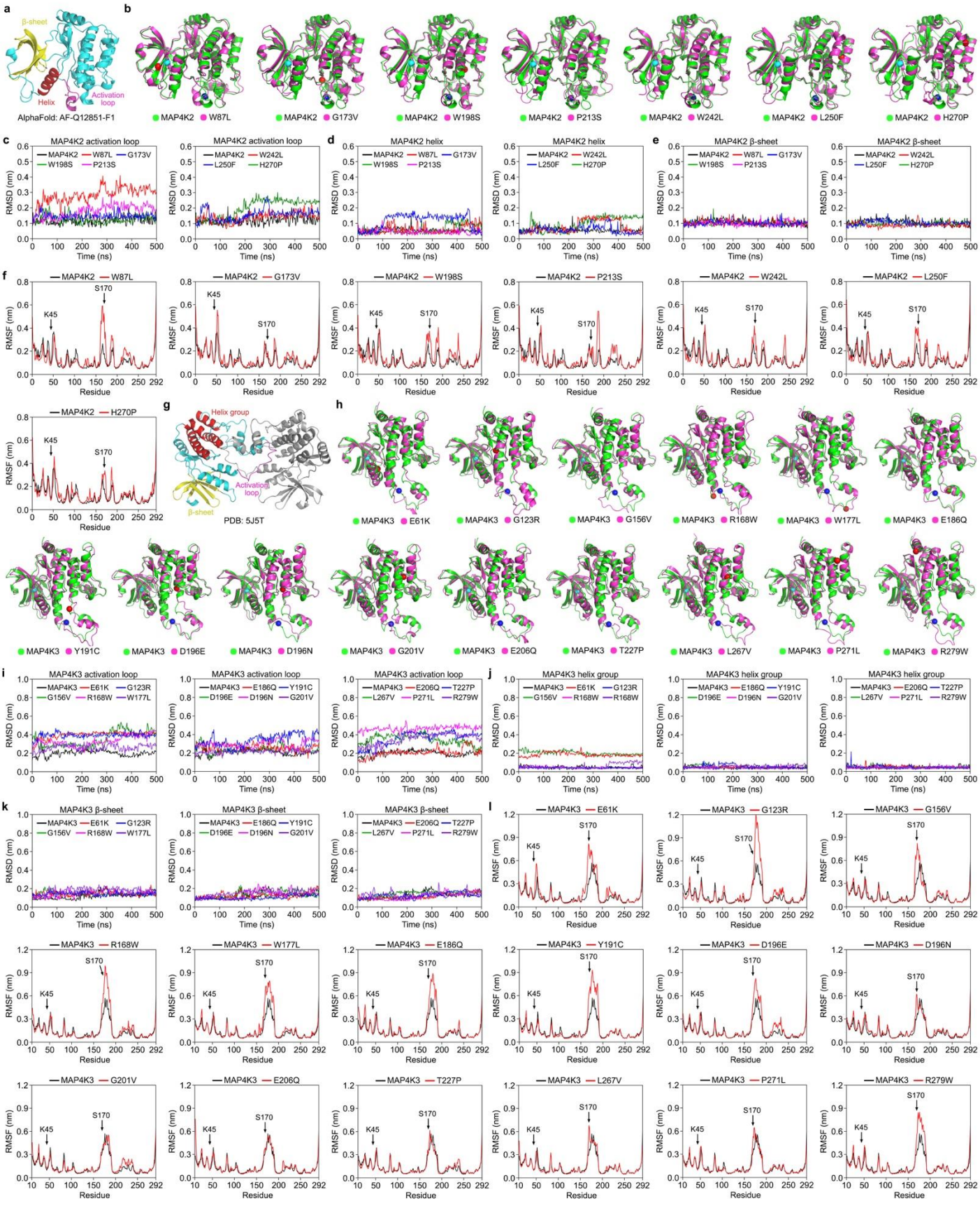
a
β-sheet
Helix
Activation loop
AlphaFold: AF-Q12851-F1
b
MAP4K2 W87L
MAP4K2 G173V
MAP4K2 W198S
MAP4K2 P213S
MAP4K2 W242L
MAP4K2 L250F
MAP4K2 H270P
c
MAP4K2 activation loop
MAP4K2 W87L G173V W198S P213S
MAP4K2 activation loop
MAP4K2 W242L L250F H270P
d
MAP4K2 helix
MAP4K2 W87L G173V W198S P213S
MAP4K2 helix
MAP4K2 W242L L250F H270P
e
MAP4K2 β-sheet
MAP4K2 W87L G173V W198S P213S
MAP4K2 β-sheet
MAP4K2 W242L L250F H270P
RMSD (nm)
Time (ns)
f
MAP4K2 W87L
MAP4K2 G173V
MAP4K2 W198S
MAP4K2 P213S
MAP4K2 W242L
MAP4K2 L250F
MAP4K2 H270P
K45
S170
RMSF (nm)
Residue
g
Helix group
Activation loop
β-sheet
PDB: 5J5T
h
MAP4K3 E61K
MAP4K3 G123R
MAP4K3 G156V
MAP4K3 R168W
MAP4K3 W177L
MAP4K3 E186Q
MAP4K3 Y191C
MAP4K3 D196E
MAP4K3 D196N
MAP4K3 G201V
MAP4K3 E206Q
MAP4K3 T227P
MAP4K3 L267V
MAP4K3 P271L
MAP4K3 R279W
i
MAP4K3 activation loop
MAP4K3 E61K G123R G156V R168W W177L
MAP4K3 activation loop
MAP4K3 E186Q Y191C D196E D196N G201V
MAP4K3 activation loop
MAP4K3 E206Q T227P L267V P271L R279W
j
MAP4K3 helix group
MAP4K3 E61K G123R G156V R168W R168W
MAP4K3 helix group
MAP4K3 E186Q Y191C D196E D196N G201V
MAP4K3 helix group
MAP4K3 E206Q T227P L267V P271L R279W
k
MAP4K3 β-sheet
MAP4K3 E61K G123R G156V R168W W177L
MAP4K3 β-sheet
MAP4K3 E186Q Y191C D196E D196N G201V
MAP4K3 β-sheet
MAP4K3 E206Q T227P L267V P271L R279W
l
MAP4K3 E61K
MAP4K3 G123R
MAP4K3 G156V
MAP4K3 R168W
MAP4K3 W177L
MAP4K3 E186Q
MAP4K3 Y191C
MAP4K3 D196E
MAP4K3 D196N
MAP4K3 G201V
MAP4K3 E206Q
MAP4K3 T227P
MAP4K3 L267V
MAP4K3 P271L
MAP4K3 R279W

**Supplementary Figure 11. Molecular dynamics analysis of the MAP4K2/3 LOF missense mutations.**

(**a**) The MAP4K2 kinase domain protein structure (predicted using AlphaFold2) is used for the molecular dynamics analysis. The activation loop, helix region, and β-sheet were shown in different colors.

(**b**) The MAP4K2 LOF missense mutations induce its kinase domain conformational change. The kinase domain overlay structures were shown for MAP4K2 and its indicated LOF missense mutants.

(**c-e**) RMSD analysis is performed to examine the MAP4K2 LOF missense mutations-caused effects on its kinase domain protein structure, where MAP4K2 kinase domain activation loop (**c**), helix group (**d**), and β-sheet (**e**) were examined.

(**f**) RMSF analysis is performed for the MAP4K2 kinase domain LOF missense mutants. MAP4K2 ATP-binding site K45 and autophosphorylation site S170 were indicated.

(**g**) The MAP4K3 kinase domain protein structure (PDB: 5J5T) is used for the molecular dynamics analysis. The activation loop, helix group, and β-sheet were shown in different colors.

(**h**) The MAP4K3 LOF missense mutations induce its kinase domain conformational change. The kinase domain overlay structures were shown for MAP4K3 and its indicated LOF missense mutants.

(**i-k**) RMSD analysis is performed to examine the MAP4K3 LOF missense mutations-caused effects on its kinase domain protein structure, where MAP4K3 kinase domain activation loop (**i**), helix group (**j**), and β-sheet (**k**) were examined.

(**l**) RMSF analysis is performed for the MAP4K3 kinase domain LOF missense mutants. MAP4K3 ATP-binding site K45 and autophosphorylation site S170 were indicated.

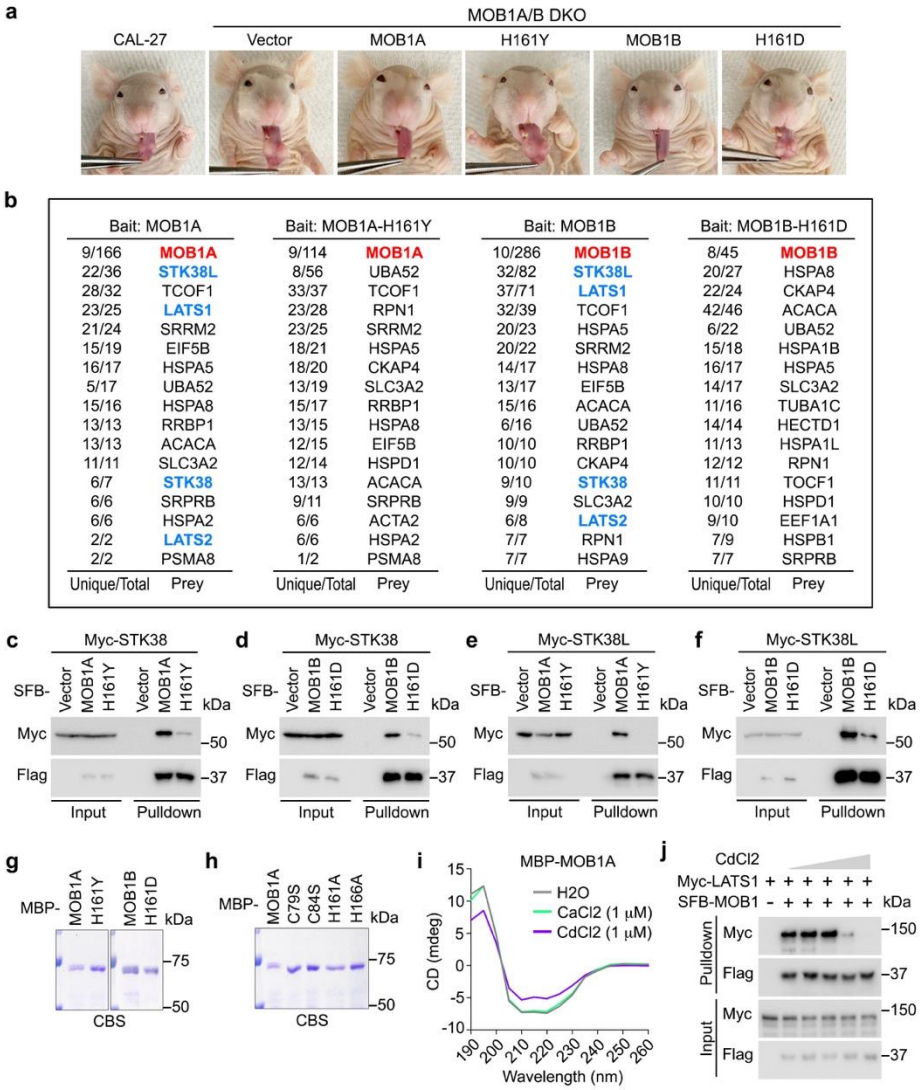
a
MOB1A/B DKO
CAL-27
Vector
MOB1A
H161Y
MOB1B
H161D
b
Bait: MOB1A
9/166 MOB1A
22/36 STK38L
28/32 TCOF1
23/25 LATS1
21/24 SRRM2
15/19 EIF5B
16/17 HSPA5
5/17 UBA52
15/16 HSPA8
13/13 RRBP1
13/13 ACACA
11/11 SLC3A2
6/7 STK38
6/6 SRPRB
6/6 HSPA2
2/2 LATS2
2/2 PSMA8
Unique/Total Prey
Bait: MOB1A-H161Y
9/114 MOB1A
8/56 UBA52
33/37 TCOF1
23/28 RPN1
23/25 SRRM2
18/21 HSPA5
18/20 CKAP4
13/19 SLC3A2
15/17 RRBP1
13/15 HSPA8
12/15 EIF5B
12/14 HSPD1
13/13 ACACA
9/11 SRPRB
6/6 ACTA2
6/6 HSPA2
1/2 PSMA8
Unique/Total Prey
Bait: MOB1B
10/286 MOB1B
32/82 STK38L
37/71 LATS1
32/39 TCOF1
20/23 HSPA5
20/22 SRRM2
14/17 HSPA8
13/17 EIF5B
15/16 ACACA
6/16 UBA52
10/10 RRBP1
10/10 CKAP4
9/10 STK38
9/9 SLC3A2
6/8 LATS2
7/7 RPN1
7/7 HSPA9
Unique/Total Prey
Bait: MOB1B-H161D
8/45 MOB1B
20/27 HSPA8
22/24 CKAP4
42/46 ACACA
6/22 UBA52
15/18 HSPA1B
16/17 HSPA5
14/17 SLC3A2
11/16 TUBA1C
14/14 HECTD1
11/13 HSPA1L
12/12 RPN1
11/11 TOCF1
10/10 HSPD1
9/10 EEF1A1
7/9 HSPB1
7/7 SRPRB
Unique/Total Prey
c
Myc-STK38
SFB- Vector MOB1A H161Y Vector MOB1A H161Y kDa
Myc
Flag
50
37
Input
Pulldown
d
Myc-STK38
SFB- Vector MOB1B H161D Vector MOB1B H161D kDa
Myc
Flag
50
37
Input
Pulldown
e
Myc-STK38L
SFB- Vector MOB1A H161Y Vector MOB1A H161Y kDa
Myc
Flag
50
37
Input
Pulldown
f
Myc-STK38L
SFB- Vector MOB1B H161D Vector MOB1B H161D kDa
Myc
Flag
50
37
Input
Pulldown
g
MBP- MOB1A H161Y MOB1B H161D kDa
75
50
CBS
h
MBP- MOB1A C79S C84S H161A H166A kDa
75
50
CBS
i
MBP-MOB1A
H2O
CaCl2 (1 μM)
CdCl2 (1 μM)
CD (mdeg)
15
10
5
0
-5
-10
190 200 210 220 230 240 250 260
Wavelength (nm)
j
CdCl2
Myc-LATS1 + + + + + +
SFB-MOB1 - + + + + + kDa
Pulldown
Myc
Flag
150
37
Input
Myc
Flag
150
37

**Supplementary Figure 12. The MOB1A/B LOF missense mutations interfere with MOB1A/B ZNF domains and protein functions.**

(**a**) The MOB1A/B LOF missense mutants promote CAL-27 xenograft tumor growth in mouse tongues. The representative images of mice and their tongues were shown.

(**b**) TAP-MS analysis of the protein-protein interaction network of MOB1A/B and their LOF missense mutants. The numbers of unique and total peptides for each identified protein were shown.

(**c-f**) The MOB1A/B LOF missense mutations disrupt the interaction of MOB1A/B with STK38 and STK38L. HEK293T cells were transfected with Myc-STK38/L and the indicated SFB-MOB1A/B constructs and subjected to pulldown assay using S protein beads. A representative blot of two independent experiments is shown.

(**g-h**) The indicated MBP-tagged MOB1A/B proteins are purified from bacteria and visualized by Coomassie blue staining (CBS).

(**i**) MOB1A protein structure is changed upon Cd treatment. The MBP-tagged MOB1A protein was incubated with 1 μM CaCl2 or CdCl2 and subjected to circular dichroism analysis.

(**j**) Cd treatment targets the MOB1-LATS1 complex formation. HEK293T cells were transfected with Myc-LATS1 and SFB-MOB1A constructs. Cell lysates were incubated with CdCl2 at different concentrations (i.e., 0 μM, 1 μM, 2.5 μM, 5 μM, and 10 μM) and subjected to pulldown assay. A representative blot of two independent experiments is shown.

Source data are provided as a Source Data file.

Supplementary Figure 13

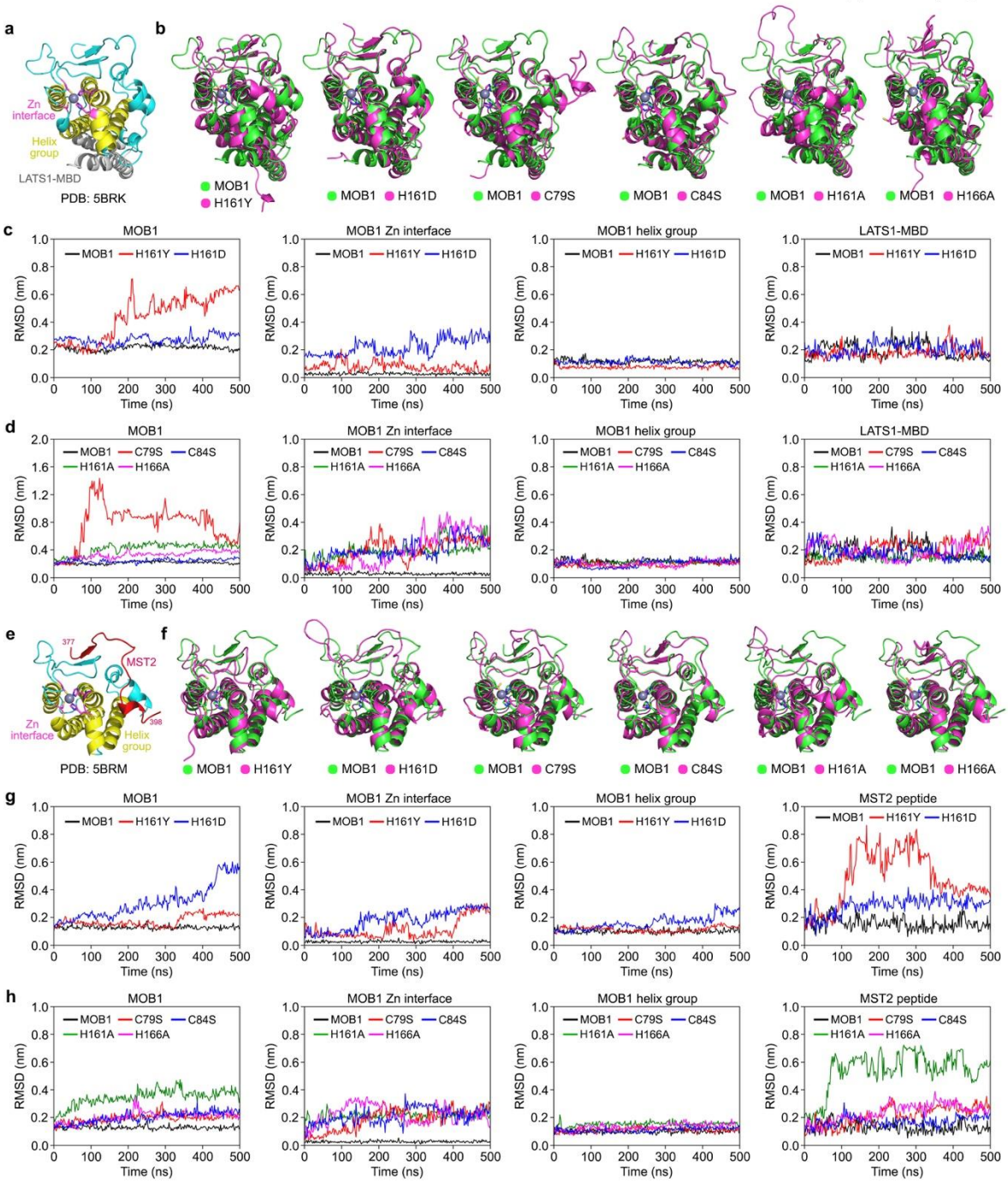

**Supplementary Figure 13. Molecular dynamics analysis of the MOB1 LOF missense mutations.**

(**a**) The p-MOB1/LATS1-MBD co-crystal structure (PDB: 5BRK) is used for the molecular dynamics analysis. The Zn interface and helix group of MOB1 and LATS1-MBD were shown in different colors.

(**b**) The MOB1 LOF and ZNF domain mutations induce the conformational change of the p-MOB1/LATS1-MBD complex. The p-MOB1/LATS1-MBD overlay structures were shown for MOB1 and its indicated LOF and ZNF domain mutants.

(**c**-**d**) RMSD analysis is performed to examine the MOB1 LOF missense mutations (**c**) and its ZNF domain mutations (**d**)-caused effects on the p-MOB1/LATS1-MBD co-crystal structure. RMSD analysis was performed for overall MOB1, its Zn interface and helix group, and LATS1-MBD within the p-MOB1/LATS1-MBD co-crystal structure.

(**e**) The MOB1/MST2-peptide co-crystal structure (PDB: 5BRM) is used for the molecular dynamics analysis. The Zn interface and helix group of MOB1 and MST2-peptide were shown in different colors.

(**f**) The MOB1 LOF and ZNF domain mutations induce the conformational change of the MOB1/MST2-peptide complex. The MOB1/MST2-peptide overlay structures were shown for MOB1 and its indicated LOF and ZNF domain mutants.

(**g**-**h**) RMSD analysis is performed to examine the MOB1 LOF missense mutations (**g**) and its ZNF domain mutations (**h**)-caused effects on the MOB1/MST2-peptide co-crystal structure. RMSD analysis was performed for overall MOB1, its Zn interface and helix group, and MST2-peptide within the MOB1/MST2-peptide co-crystal structure.

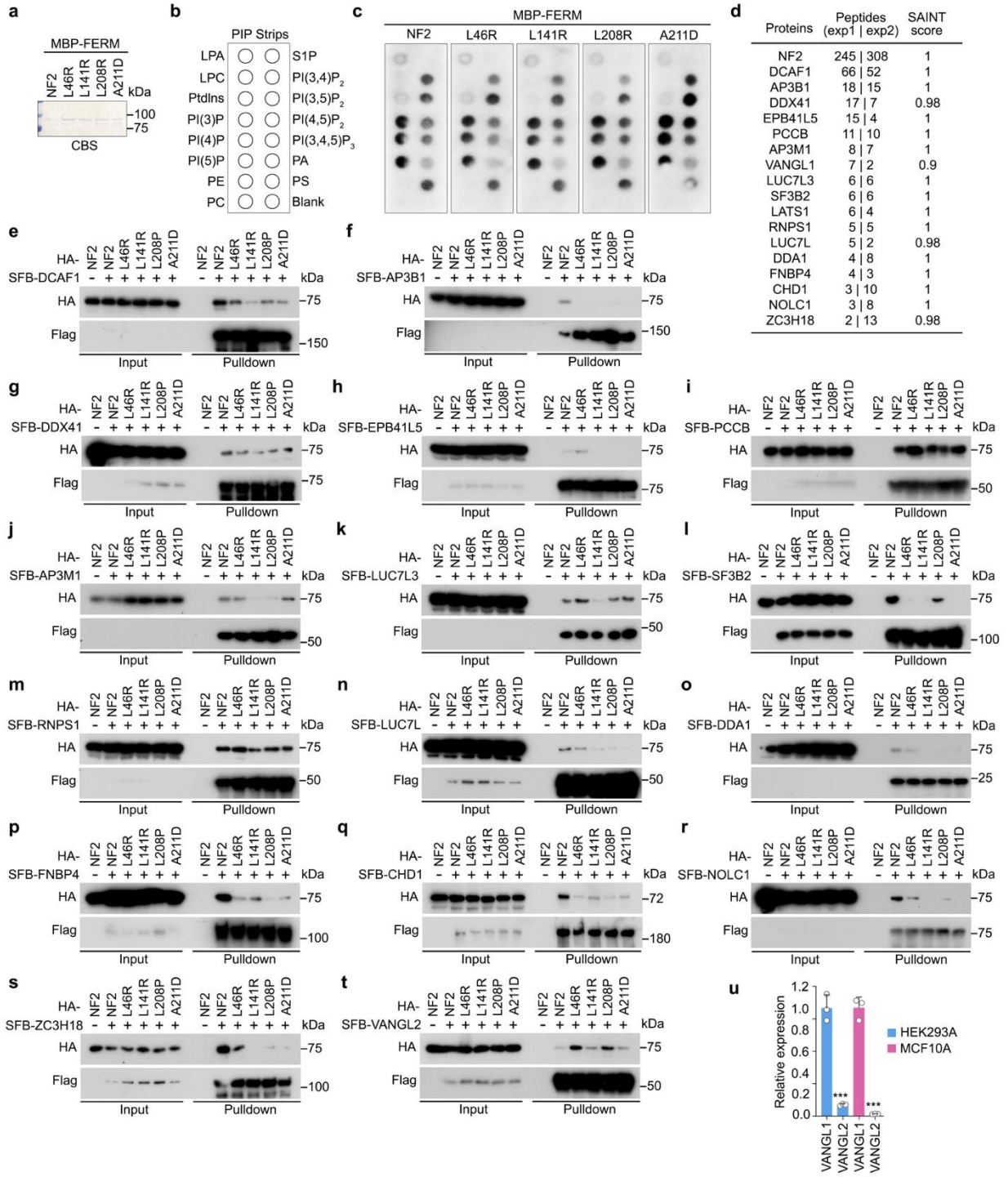
a
MBP-FERM
NF2
L46R
L141R
L208R
A211D
kDa
100
75
CBS
b
PIP Strips
LPA
LPC
PtdIns
PI(3)P
PI(4)P
PI(5)P
PE
PC
S1P
PI(3,4)P2
PI(3,5)P2
PI(4,5)P2
PI(3,4,5)P3
PA
PS
Blank
c
MBP-FERM
NF2
L46R
L141R
L208R
A211D
d
Proteins | Peptides (exp1 | exp2) | SAINT score
NF2 | 245 | 308 | 1
DCAF1 | 66 | 52 | 1
AP3B1 | 18 | 15 | 1
DDX41 | 17 | 7 | 0.98
EPB41L5 | 15 | 4 | 1
PCCB | 11 | 10 | 1
AP3M1 | 8 | 7 | 1
VANGL1 | 7 | 2 | 0.9
LUC7L3 | 6 | 6 | 1
SF3B2 | 6 | 6 | 1
LATS1 | 6 | 4 | 1
RNPS1 | 5 | 5 | 1
LUC7L | 5 | 2 | 0.98
DDA1 | 4 | 8 | 1
FNBP4 | 4 | 3 | 1
CHD1 | 3 | 10 | 1
NOLC1 | 3 | 8 | 1
ZC3H18 | 2 | 13 | 0.98
e
SFB-DCAF1
f
SFB-AP3B1
g
SFB-DDX41
h
SFB-EPB41L5
i
SFB-PCCB
j
SFB-AP3M1
k
SFB-LUC7L3
l
SFB-SF3B2
m
SFB-RNPS1
n
SFB-LUC7L
o
SFB-DDA1
p
SFB-FNBP4
q
SFB-CHD1
r
SFB-NOLC1
s
SFB-ZC3H18
t
SFB-VANGL2
HA-
NF2
L46R
L141R
L208P
A211D
kDa
HA
Flag
Input
Pulldown
u
Relative expression
HEK293A
MCF10A
VANGL1
VANGL2
***

**Supplementary Figure 14. The NF2 LOF mutations do not affect NF2 lipid-binding ability but promote its interaction with VANGL proteins.**

(**a**) The indicated MBP-tagged NF2 FERM proteins are purified from bacteria and visualized by Coomassie blue staining (CBS).

(**b**) Illustration of the PIP Strips membrane used for the protein-lipid interaction study.

(**c**) The NF2 LOF mutations do not affect the interaction of NF2 FERM domain with the phospholipids. The PIP Strips membranes were incubated with the bacterially purified MBP-tagged NF2 FERM domain mutant proteins and subjected to Western blot. A representative blot of two independent experiments is shown.

(**d**) Summary of the NF2 HCIPs identified through two biologically repeated TAP-MS analyses. The total peptide number and SAINT score for each HCIP were shown.

(**e-s**) Characterization of the NF2 LOF mutations-caused effects on the interaction of NF2 with its HCIPs. HEK293T cells were transfected with HA-NF2 LOF mutants and the indicated SFB-tagged HCIPs and subjected to pulldown assay using S protein beads. A representative blot of two independent experiments is shown.

(**t**) The NF2 LOF mutations promote its interaction with VANGL2. HEK293T cells were transfected with HA-NF2 LOF mutants and SFB-VANGL2 and subjected to pulldown assay. A representative blot of two independent experiments is shown.

(**u**) *VANGL2* is lowly expressed in HEK293A and MCF10A cells as compared to *VANGL1*. The transcription of *VANGL1* and *VANGL2* was examined by q-PCR (mean ± s.d., n = 3 biological replicates). *** $p < 0.001$ (two-tailed Student's *t*-test).

Source data are provided as a Source Data file.

## Uncropped scans of all blots and gels

Supplementary Figure 6

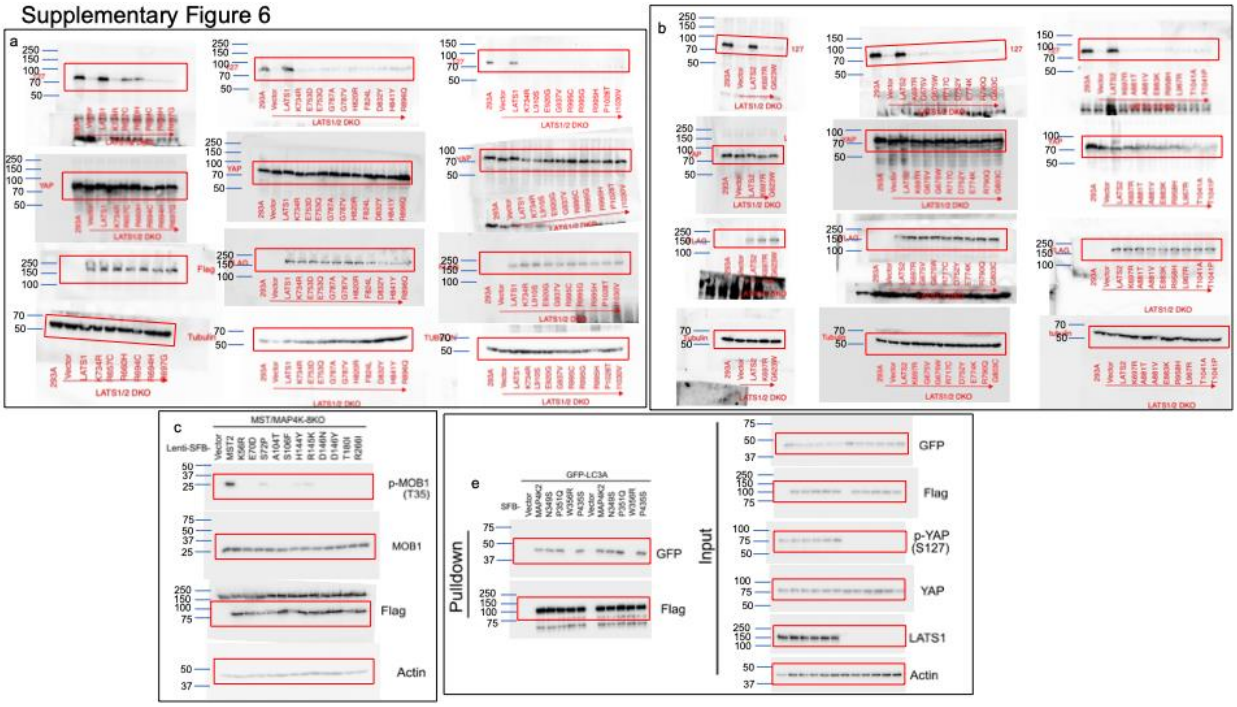


Supplementary Figure 12

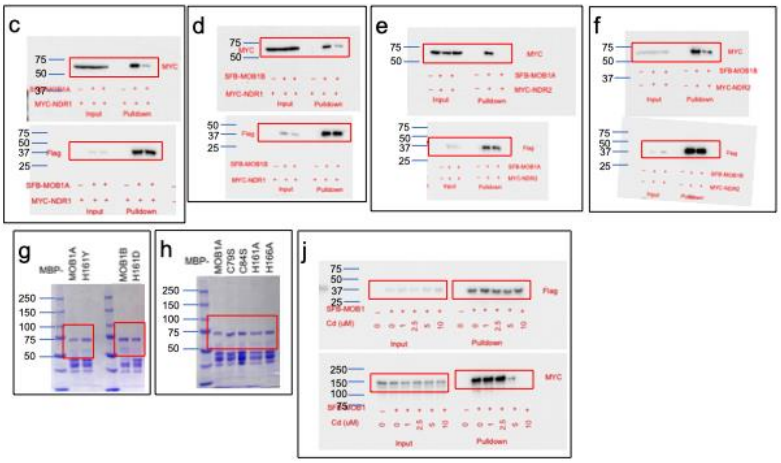

Supplementary Figure 14